Rivet Graphene

Xinlu Li,[*,†,≠] *Junwei Sha,*[†,⊥,#] *Seoung-Ki Lee,*[†] *Yilun Li,*[†] *Yongsung Ji*[†]*, Yujie Zhao*[≠]*, and James M.*

Tour[*,†,‡,§]

[†]*Department of Chemistry,* [‡]*NanoCarbon Center,* [§]*Department of Materials Science and*

NanoEngineering, Rice University, 6100 Main Street, Houston, Texas 77005, United States

[≠]*School of Materials Science and Engineering, Chongqing University, Chongqing 400030,*

China; [⊥]*School of Materials Science and Engineering, Tianjin Key Laboratory of Composite and*

Functional Materials, Tianjin University, Tianjin 300072, China; [#]*Collaborative Innovation*

Center of Chemical Science and Engineering, Tianjin 300072

*E-mail: lixinlu@cqu.edu.cn, tour@rice.edu

Abstract Large-area graphene has emerged as a promising material for use in flexible and

transparent electronics due to its flexibility and optical and electronic properties. The anchoring

of transition metal nanoparticles on large-area single-layer graphene is still a challenge. Here we

report an *in situ* preparation of carbon nano-onion-encapsulated Fe nanoparticles on rebar

graphene, which we term rivet graphene. The hybrid film, which allows for polymer-free transfer

and is strong enough to float on water with no added supports, exhibits high optical transparency,

excellent electric conductivity and good hole/electron mobility under certain tensile/compressive

strains. The results of contact resistance and transfer length indicate that the current in the rivet

1

1
2
3
4
5
6
7
8
9
10
11
12
13
14
15
16
17
18
19
20
21
22
23
24
25
26
27
28
29
30
31
32
33
34
35
36
37
38
39
40
41
42
43
44
45
46
47
48
49
50
51
52
53
54
55
56
57
58
59
60

graphene transistor does not just flow at the contact edge. Carbon nano-onions encapsulating Fe nanoparticles on the surface enhance the injection of charge between rivet graphene and the metal electrode. The anchoring of Fe nanoparticles encapsulated by carbon nano-onions on rebar graphene will provide additional avenues for applications of nanocarbon-based films in transparent and flexible electronics.

Keywords Fe nanoparticles, nano-onions, rebar graphene, carbon nanotubes, hybrid film

Graphene has been intensively studied due to its outstanding properties and potential applications in flexible electronics, high frequency transistors and logic devices. Currently, the growth of large-area monolayer graphene by chemical vapor deposition (CVD) on transition metal substrates and transfer to other substrates with the assistance of a stronger polymer overlayer is regarded as the most promising scalable synthesis route in industrial applications.[1,2] However, the electrical properties of graphene are diminished by the unavoidable polymer contaminants on the surface of graphene that cannot be thoroughly removed in a transfer process. In addition, large-area monolayer graphene easily cracks due to its polycrystalline nature.[2] The mechanical strength of large-area graphene needs to be improved.[3-5]

Rebar graphene, in which carbon nanotubes (CNTs) interconnect in an in-plane network to reinforce monolayer graphene, allows for polymer-free transfer and suspension on water.[6,7] With the improved mechanical strength, rebar graphene could be a good platform for flexible

electronics, and if transition metal nanoparticles can be anchored on the surface, further applicability might be realized.

Here, we report on an *in situ* preparation of carbon nano-onions (CNOs) encapsulating Fe nanoparticles (Fe@CNOs) on the surface of large-area SWCNT-reinforced rebar graphene by a facile and potentially scalable CVD method. The rebar graphene is strong enough to act as a substrate to support the Fe@CNOs. The Fe nanoparticles are protected from air oxidation by the CNO shells, and firmly fixed on the rebar graphene through covalent connections between the graphene underlayers and CNOs. The structure of Fe@CNOs on rebar graphene is similar to rivet joints in metals, therefore we refer to this as "rivet graphene". The rivet graphene is strong enough to allow for polymer-free transfer and the hybrid material floats on water without breaking, similar to rebar graphene,[6] characteristics that will aid in transfer and use as an electrocatalyst. In addition, the anchoring of Fe@CNOs on rebar graphene improves the electrical properties and subsequent potential applications in transparent and flexible electronics.

Results and Discussion

Figure 1 illustrates the two CVD steps to synthesize rivet graphene in a facile and scalable way. The single-walled carbon nanotubes (SWCNTs) were synthesized in the Rice HiPco Laboratory.[8] In the first CVD step, SWCNTs (7.0 mg) were dispersed and tip-sonicated in a Pluronic F127 aqueous solutions (10 mL, 1.0 mg/mL) at 80 W for 15 min. Surfactant-wrapped SWCNT solutions (50 µL) were spin-coated 10 successive times at 1000 rpm for 30 s each on a pretreated Cu foil (1 × 1 cm). Then the Cu foil was positioned in the central chamber of a CVD

furnace and annealed at 1070 °C in a H_2/CH_4 gas flow (300/10 sccm) for 20 min. After the

annealing step, the Cu foil was quickly removed from the hot chamber and cooled to room

temperature to afford rebar graphene on Cu. In the second CVD step, a 50 µL solutions of Fe_3O_4

nanoparticles in hexane was spin-coated on the rebar graphene-covered Cu foil 5 successive

times at 1000 rpm for 30 s each. The synthesis of Fe_3O_4 nanoparticles in the size range from ~ 20

to 40 nm is given in the Methods section. The foil was put in the central chamber of the CVD

furnace again and annealed at 850 °C in the H_2/CH_4 gas flow (500/10 sccm) for 15 min. After

annealing, the Cu foil was quickly removed from the hot chamber and cooled to room

temperature. Then the bottom face of the Cu foil was etched by an oxygen reactive-ion plasma

cleaner. The Cu foil was placed on an etching solution to remove the Cu substrate without any

polymer support. The etching solution was composed of $(NH_4)_2S_2O_3$, 1-butanol and H_2O in the

ratio of 10 g:10 mL:1000 mL.
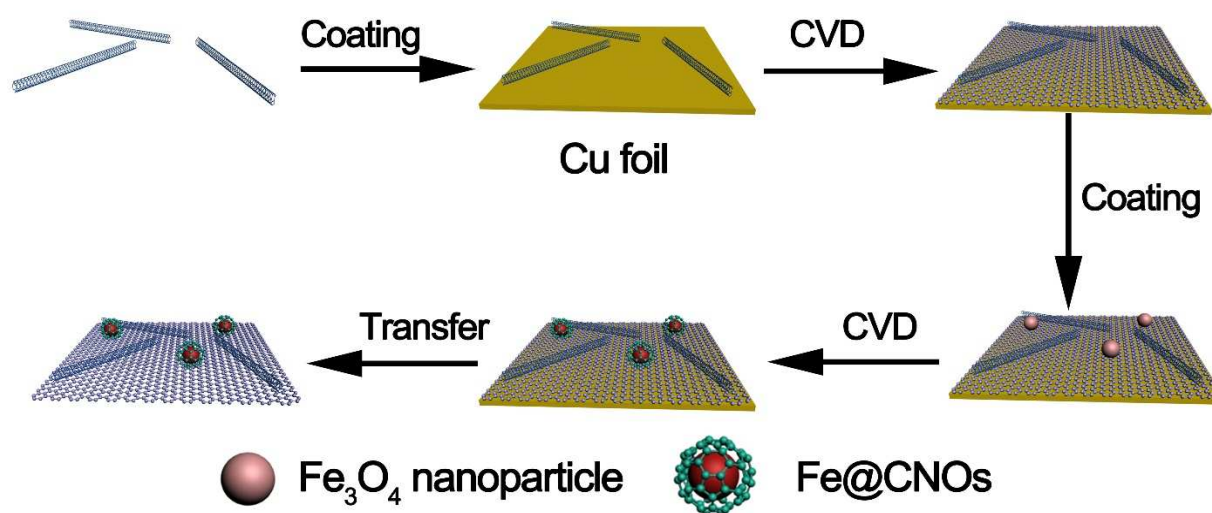
Figure 1. The synthesis of rivet graphene using a process including two CVD steps. A Cu foil (1

× 1 cm) was spin-coated with a surfactant-wrapped SWCNT aqueous solution and graphene was

4

1
2
3
4
5
6
7
8
9
10
11
12
13
14
15
16
17
18
19
20
21
22
23
24
25
26
27
28
29
30
31
32
33
34
35
36
37
38
39
40
41
42
43
44
45
46
47
48
49
50
51
52
53
54
55
56
57
58
59
60

grown on the Cu foil in the first CVD step using a methane/hydrogen mixture. The Fe_3O_4

nanoparticles were spin-coated on top of the rebar graphene and the assembly was subjected to a

second CVD process using a methane/hydrogen mixture. The resulting rivet graphene was

transferrable to other substrates.
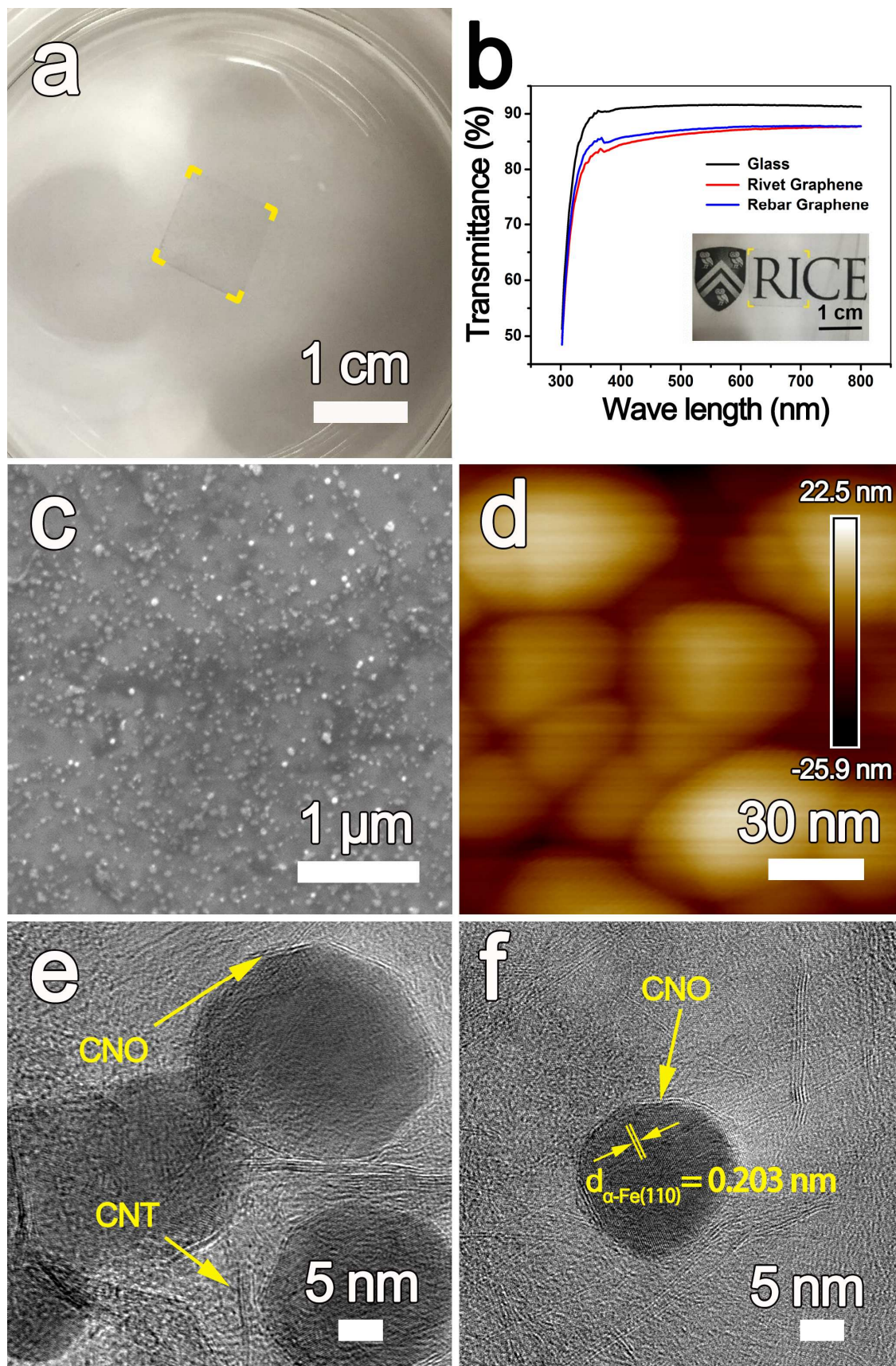
Figure 2. (a) A photograph of rivet graphene, with its corners indicated by the yellow marks, floating on water containing 1% 1-butanol. (b) UV-Vis spectra of the glass slide by itself, rebar graphene and rivet graphene on the glass slide without any polymer overlay. The inset is a photograph of rivet graphene on the glass slide; the corners of the rivet graphene are indicated by the yellow marks. (c) A SEM image of rivet graphene on a SiO_2/Si wafer, showing the distribution of Fe@CNOs on the surface of rebar graphene. (d) An AFM image of rivet graphene on a SiO_2/Si wafer; the size of individual Fe@CNOs is ~ 30 nm. (e, f) TEM images of rivet graphene that show the Fe@CNOs with 2 to 3 graphene shells encapsulating the ~ 30 nm Fe nanoparticles on the rebar graphene.

In Figure 2a, a rivet graphene film was transferred atop water containing 1% 1-butanol without using a polymer overlayer and floated without breaking. Figure 2b shows UV-Vis spectra of the glass slide by itself, rebar graphene and rivet graphene on the glass slide; the optical transmittance of rebar graphene is 95.4% at 550 nm, which is consistent with our previous result (95.6%).[6] The transmittance of rivet graphene is decreased to 94.8%, which is slightly less than in that of rebar graphene. The decrease of transmittance is presumably caused by the optical absorbance of the Fe@CNOs on the surface of the rebar graphene. The inset in Figure 2b is a photograph of rivet graphene on a glass slide. Figure 2c is a typical SEM image of rivet graphene on a SiO_2/Si wafer. There are nanoparticles on the surface, indicating Fe@CNOs are adhered to the rebar graphene. Figure 2d is a tapping mode atomic force microscope (AFM)

7

image of rivet graphene, showing that the diameter of CNOs is ~ 30 to 40 nm. Figures 2e,f are

transmission electron microscope (TEM) images of rivet graphene. In Figure 2e, the spherical

CNO shells encapsulate the 20 to 30 nm Fe nanoparticles with 2 to 4 graphene layers and are

adhering to the hybrid film. It should be noted that the CNO shells are discontinuous on the

surface of Fe nanoparticles at the joints of crystal planes, where graphene can be formed and

deposited, as shown in Figure 2e. Individually dispersed SWCNTs are observed within the

surface of rivet graphene. The marked SWCNT with one part of a sidewall gone while the other

remains are indications that rebar graphene, with SWCNTs and graphene seemlessly welded

together, is synthesized.[6,7] In Figure 2f, the well-dispersed SWCNTs formed an interconnected

network on the continuous graphene, and this is compared to the SEM and TEM images of

iron-free rebar graphene in Figure S3. As a result, the networked SWCNT-based rebar graphene

acts as a robust substrate for Fe@CNOs after the second CVD step that can be transferred to

water containing 1% butanol without assistance from a polymer overlay. According to the X-ray

diffraction (XRD) pattern of Fe nanoparticles in Figure S1, the interlayer of Fe lattice fringe was

defined as the d (110) of α-Fe, which was measured to be 0.203 nm.

8
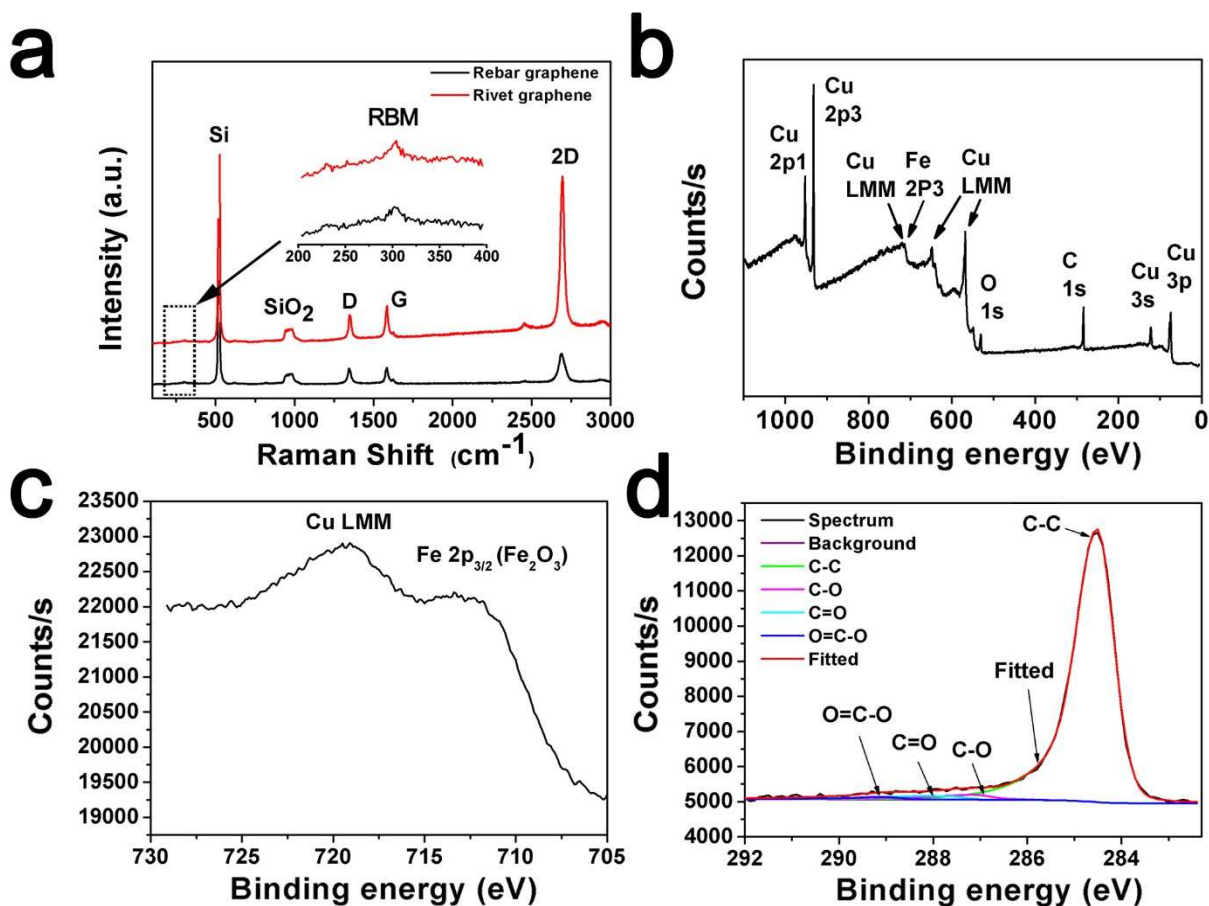
Figure 3. (a) Raman spectra of rebar and rivet graphene. The inset shows the RBM of SWCNTs in both samples. The monolayer graphene is indicated by the intensity ratio of 2D/G (~ 4.4) and the sharp 2D peak. The spectra also indicate the D/G intensity ratios of rebar graphene (0.94) and rivet graphene (0.75). (b) XPS survey scan of rivet graphene showing the elemental composition; the sample was mounted on Cu foil. (c,d) XPS showing the Fe $2p_{3/2}$ peak and the dominant sp^2 C in rivet graphene.

Raman spectroscopy was used to compare the structure of SWCNT-based rebar graphene and rivet graphene on a SiO_2/Si wafer. The Raman spectra in Figure 3a are characteristic of 10

9

locations recorded on 1 cm^2 of the sample. Both rebar graphene and rivet graphene exhibit four

typical bands: radical breathing modes (RBMs) at ~ 300 cm^{-1}, a weak D band at ~ 1350 cm^{-1}, a G

band at ~ 1582 cm^{-1} and a 2D band at ~ 2690 cm^{-1}. The RBMs substantiate the existence of

single-walled CNTs in both of the hybrid films.[6] The intensity ratio of D to G bands of

SWCNT-based rebar graphene was measured to be 0.94, which is higher than that of 0.75 for

rivet graphene, indicating the graphitic content of rivet graphene was improved and more defects

were self-healed. Because the rivet graphene was prepared by two CVD steps at high

temperature, and afterward annealed in the same CH_4/H_2 gas flow, structural defects and

disordered carbon were better healed. Furthermore, with the increase of annealing time at high

temperature (850 °C), there is increased likelihood that unzipped CNTs would self-heal and

merge into the graphene layer.[6,7] Consequently, the graphitic content of rivet graphene is

improved compared to that in rebar graphene. A single sharp 2D band appeared in both rebar

graphene and rivet graphene Raman spectra, indicating the dominant monolayer nature of the

graphene. In the case of rivet graphene, the intensity of the 2D band is much sharper than in

rebar graphene, indicating an improvement in the monolayer graphene sheet. The peak intensity

ratio of 2D to G bands in Raman spectra has been widely used to define the layer number of

graphene.[9-12] Consistent with rebar graphene, the peak ratio I_{2D}/I_G of rivet graphene is ~ 4.4,

which indicates the number of graphene layers is likely one. Based on the TEM image in Figure

S2, the graphene sheet beneath the SWCNTs and CNOs in the rivet graphene is monolayer.

To characterize the elemental composition, X-ray photoelectron spectroscopy (XPS) spectra

10

were taken of the rivet graphene on Cu foils. According to the survey spectrum in Figure 3b, the

atomic concentration of the rivet graphene in the scanned surface is 64.7% C 1s, 13.3% Fe 2p3

and 22.0% O1s. After calibration, the Fe is deconvoluted to Fe(III) $2p_{3/2}$ at 711.66 eV, as shown

in Figure 3c.[13,14] In the second CVD process, a hexane solution of Fe_3O_4 nanoparticles was

spin-coated on the surface of rebar graphene. Under the flow of CH_4/H_2 gas at 850 °C, most of

the Fe_3O_4 nanoparticles were reduced to Fe nanoparticles, which were used as the catalyst for

CNO growth. These Fe nanoparticles were encapsulated by CNOs and fixed on rebar graphene.

After exposure to air for a few days, the Fe nanoparticles were oxidized to form α-Fe_2O_3.

Moreover, the Fe 2p3/2 peak of Fe metal is not obvious in the XPS analysis due to the intense

overlapping Cu LMM peak. But the existence of Fe metal can be confirmed based on the TEM

and XRD analyses. In Figure 3d, the fitting standard for C 1s peak of graphene was shifted to

284.5 eV due to the conjugative effect of sp^2 C. The sharpest sp^2 C peak at 284.56 eV is

asymmetric due to the C-C conjugative effect in graphene, indicating that the dominant sp^2 C is

due to the graphene structure in the hybrid film. The carbon in SWCNTs with unzipped parts or

in CNO shells have some oxygenated bonds, such as C-O, C=O or O=C-O bonds, resulting in

disordered carbon or defects.[15] The obvious D band in the Raman spectra as shown in Figure 3a

further confirmed the phenomenon.
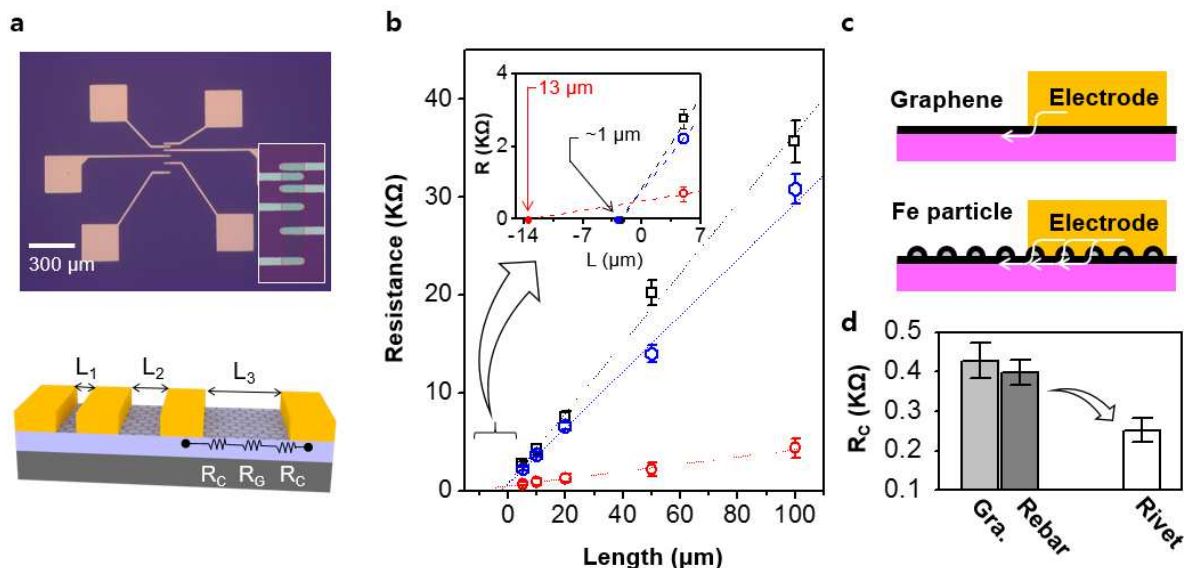
Figure 4. (a) (top) A photo image and (bottom) schematic diagram of the Si-based transistor; the inset in the top photo shows that rivet graphene is located on Au electrodes. (b) Calculation of the contact resistance between rivet graphene and a Au electrode (red line). As control samples, the contact resistance of normal graphene and rebar graphene are shown by the black and blue lines, respectively. The inset shows the transfer length of the rivet graphene (13 µm) and normal graphene (1 µm). (c) Schematic diagram of the current flow between rivet graphene and the metal electrode, as compared to the control sample made using normal graphene. (d) The contact resistance of rivet graphene is ~ 40% lower than in normal graphene as well as rebar graphene.


    To determine the advantages of the unique structure of rivet graphene, having Fe nanoparticles encapsulated by CNOs, we fabricated a multi-probe device with different channel lengths, known as the transfer length method (TLM).[16] Devices composed of single-layer graphene as well as rebar graphene were also fabricated as control samples. An optical

12

microscope image and schematic of the TLM test device is shown in Figure 4a. The distance

between contacts was varied from 5, 10, 20, 50 to 100 μm and the width of each contact was

fixed at 100 μm. After measuring the total resistance between adjacent contacts, the contact

resistance (R_C) was calculated using eq 1:

$$R_T = 2R_M + 2R_C + R_G \ (1)$$

where R_T is the total resistance between the source and drain; R_M is the resistance due to the

contact metal; R_G is the resistance of rivet graphene between the two voltage probes; and R_C is

associated with the metal/rivet graphene interface.[17,18] Since the resistivity of the metal in the

contact is quite low, where $R_G \gg R_M$, R_M was ignored in this calculation. The measured total

resistance (R_T) was plotted against the channel length in Figure 4b. The contact resistance (R_C) is

calculated from the extrapolated value of resistance at zero contact spacing (at L= 0 μm). The

calculated R_C clearly show that the R_C of the device from rivet graphene, 252 ± 51 Ω, is ~ 40%

lower than that of the control devices at 427 ± 57 Ω and 396 ± 32 Ω from graphene and rebar

graphene, respectively. In addition, the TLM can determine the transfer length (L_T), indicating

the distance over which the current flows from the graphene semiconductor to the metal

electrode or *vice versa*. The $2L_T$ can be calculated at R = 0 as shown in the inset of Figure 4b.

For the graphene sample, one of the control devices, the transfer length is ~ 0.5 μm, which agrees

well with previous reports.[17,18] Interestingly, in the case of rebar graphene, the transfer length

showed no significant change ($L_T \sim 1$ μm), while the L_T of rivet graphene was dramatically larger

at ~ 6.5 μm. These two results, contact resistance and transfer length, indicate that the current in

the rivet graphene device does not just flow at the contact edge (Figure 4c). In addition, we postulate that the Fe nanoparticles or the edge sites of CNOs enhance the injection of charge between graphene and the metal electrode from the comparison of results from rebar graphene and rivet graphene (Figures 4b and 4d).[19-21]
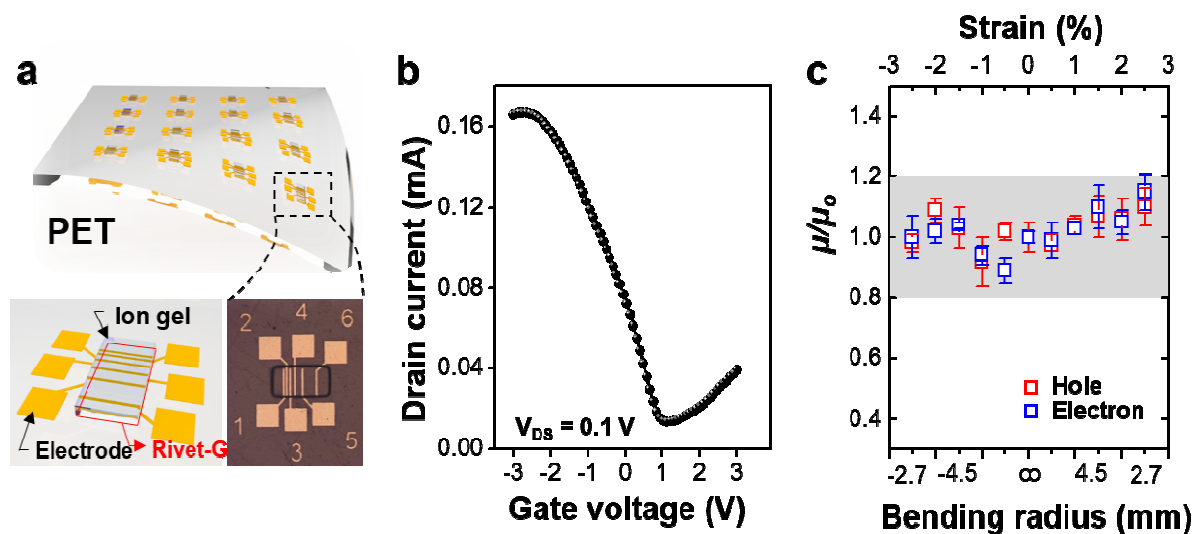
Figure 5. (a) Schematic diagram of ion gel gated rivet graphene transistors on a PET substrate. Bottom left image: schematic illustration of unit cell; bottom right image: optical microscope image of the transistor. (b) Transfer characteristics (I_D *vs* V_G) of rivet graphene at $V_{DS} = 0.1$ V. The positive Dirac voltage ($V_D = 1$ V) means the Fe nanoparticle as well as CNOs work as acceptors on graphene (*p*-type behavior). (c) The normalized hole/electron mobilities of rivet graphene as a function of bending radius. The rivet graphene maintains its electrical properties up to 2.5% of compression and tensile stress. At this strain level, the bending radius of the substrate is 2.7 mm. The rivet graphene shows excellent bendability for its application in flexible electronics.

14

Furthermore, to analyze the electromechanical properties of rivet graphene, a thin film transistor (TFT) was fabricated on a plastic substrate. A schematic illustration of the rivet graphene-based TFT is shown in Figure 5a together with an optical image of one of the transistors. After transfer of the rivet graphene onto the 70 μm-thick PET substrate, source and drain Au electrodes (50 nm) were deposited on top of the rivet graphene film using photolithography and e-beam evaporation. For use as a flexible gate dielectric, UV-crosslinkable ion gel ink containing a radical initiator 2-hydroxy-2-methylpropiophenone, poly(ethylene glycol) diacrylate monomer, and the 1-ethyl-3-methylimidazolium bis(trifluoromethylsulfonyl)imide [EMIM:TFSI] ionic liquid (the weight ratio of 8:4:88) was drop-cast and exposed to UV light, 100 mW/cm^2 at 365 nm.[22] The graphene not covered by the ion gel was removed using oxygen plasma. The capacitance of the UV-patterned ion gel on the PET substrate was 7.29 μF/cm^2 at 10 Hz. Figure 5b shows the typical transfer curve of the flexible rivet graphene TFTs, which is measured within the range of gate voltage (V_{GS}) from -3 V to 3 V at a fixed drain voltage (V_{DS}) of 0.1 V. Using these results, we derived the hole and electron mobility of graphene devices using eq. 2:[23]

$$\left|V_G - V_{G,min}\right| = {hv_F\sqrt{\pi n}}/{e} + {ne}/{C_{EDL}} \quad (2)$$

where h is Planck's constant, v_F is the Fermi velocity, n is the charge density, and e is the electron charge. The calculated conductivity was plotted as a function of charge density in Figure S4. The average carrier mobilities for holes and electrons were 132 cm^2/Vs and 28 cm^2/Vs,

15

respectively (Figure 5b). The mechanical strength was further tested by performing the same

measurements under both compressive as well as tensile strain. For this purpose, devices were

bent to a variable radius of curvature (r) and the mobility of each state was measured as a

function of strain (or bending radii).

Figure 5c summarizes the variation in relative mobility, μ/μ_0, where μ and μ_0 are the mobility

at bending state and under the flat state, respectively, as a function of tensile as well as

compressive strains. The results show that transistor maintains its electrical characteristics up to

2.5 mm regardless of tensile/compressive strains (*i.e.* strain of 2.8%), which would be sufficient

for many flexible applications.

To confirm the importance of the Fe in the rivet graphene, we removed the Fe nanoparticles

by hydrochloric acid etching and produced an inferior graphene film that was so weak that it was

easy to break when transferred from the acid etching solution to water. Figure S5 shows TEM

images of the rivet graphene after removal of the Fe nanoparticles. Many cracks and holes

occurred in the graphene after the Fe removal.

Conclusions

Rivet graphene was synthesized using a facile and potentially scalable CVD method. In rivet

graphene, Fe nanoparticles encapsulated CNOs core-shell structure was grown *in situ* on the

surface of large-area SWCNT-reinforced rebar graphene. The composite film exhibits many

unique properties, such as enabling polymer-free transfer, high optical transparency, and *p*-type

16

1
2
3
4
5
6
7
8
9
10
11
12
13
14
15
16
17
18
19
20
21
22
23
24
25
26
27
28
29
30
31
32
33
34
35
36
37
38
39
40
41
42
43
44
45
46
47
48
49
50
51
52
53
54
55
56
57
58
59
60

behavior in a PET TFT. The anchoring of Fe nanoparticles encapsulated by CNOs on rebar

graphene can effectively reduce the contact resistance and maintain high hole/electron mobility

under 2.8% tensile/compressive strains, providing an approach to potential applications in

transparent and flexible electronics.

Methods

Synthesis of Fe₃O₄ nanoparticles. Fe_3O_4 nanoparticles were synthesized by a simple reflux

method.[24] In brief, iron(III) acetylacetonate (0.15 g), 1,2-hexadecanediol (0.616 g), oleylamine

(0.62 mL), and oleic acid (0.45 mL) were added to 20 mL benzyl ether under magnetic stirring

(500 rpm). Then the mixture was heated to reflux at 200 °C for 20 min. After cooling to room

temperature, the nanoparticles were collected by adding 20 mL of methanol and centrifuging at

4000 rpm for 5 min. After repeating the centrifugation three times, the nanoparticles were

dispersed in hexane (20 mL) under ultrasonication. The optimum concentration of the dispersion

was ~ 0.4 mg mL^{-1}.

Sample characterization. The Raman spectra were recorded with a Renishaw Raman RE01

scope. SEM image were observed using a JEOL 6500F Scanning Electron Microscope. TEM

images were taken using a 200 kV JEOL FE2100 Transmission Electron Microscope. AFM

images were obtained on a Digital Instrument Nanoscope IIIA. XPS was performed on a PHI

Quantera SXM scanning X-ray microprobe with 100 μm beam size and 45° takeoff angle.

17

Supporting Information Available: Includes materials, methods and additional graphs. This material is available free of charge *via* the Internet at http://pub.acs.org.

References and Notes

1. Liu, Y.; Wang, F.; Wang, X. M.; Wang, X. Z.; Flahaut, E.; Liu, X.; Li, Y.; Wang, X. R.; Xu, Y. B.; Shi, Y.; Zhang, R. Planar Carbon Nanotube-Graphene Hybrid Films for High-Performance Broadband Photodetectors. *Nat. Commun.* **2015**, *6*, 8589.

2. Lin, X. Y.; Liu, P.; Wei, Y.; Li, Q. Q.; Wang, J. P.; Wu, Y.; Feng, C.; Zhang, L.; Fan, S. S.; Jiang, K. L. Development of an Ultra-Thin Film Comprised of a Graphene Membrane and Carbon Nanotube Vein Support. *Nat. Commun.* **2013**, *4*, 2920.

3. Liu, W. Q.; Wang, W. Y.; Wang, J. J.; Wang, F. Q.; Lu, C.; Jin, F.; Zhang, A.; Zhang, Q. M.; Laan, G.; Xu, Y. B.; Li, Q. X.; Zhang, R. Atomic-Scale Interfacial Magnetism in Fe/Graphene Heterojunction. *Sci. Rep.* **2015**, *5*, 11911.

18

4. Boukhvalov, D.; Gornostyrev, Y.; Uimin, M.; Korolev, A.; Yermakov, A. Atomic, Electronic and Magnetic Structure of Graphene/Iron and Nickel Interface: Theory and Experiment. *RSC Adv.* **2015**, *5*, 9173-9179.

5. Rani, J.; Oh, S.; Woo, J.; Jang, J. Low Voltage Resistive Memory Devices Based on Graphene Oxide-Iron Oxide Hybrid. *Carbon* **2015**, *94*, 362-368.

6. Yan, Z.; Peng, Z. W.; Casillas, G.; Lin, J.; Xiang, C. S.; Zhou, H. Q.; Yang, Y.; Ruan, G. D.; Raji, A-R. O.; Samuel, E. L. G.; Hauge, R. H.; Jose-Yacaman, M.; Tour, J. M. Rebar Graphene. *ACS Nano* **2014**, *8*, 5061-5068.

7. Li, Y. L.; Peng, Z. W.; Larios, E.; Wang, G.; Lin, J.; Yan, Z.; Ruiz-Zepeda, F.; Jose-Yacaman, M.; Tour, J. M. Rebar Graphene from Functionalized Boron Nitride Nanotubes. *ACS Nano* **2015,** *9*, 532-538.

8. Nikolaev, P.; Bronikowski, M. J.; Bradley, R. K.; Rohmund, F.; Colbert, D. T.; Smith, K. A.; Smalley, R. E. Gas-Phase Catalytic Growth of Single-Walled Carbon Nanotubes from Carbon Monoxide. *Chem. Phys. Lett.* **1999**, *313*, 91-97.

9. Li, X.; Cai, W.; An, J. H.; Kim, S.; Nah, J.; Yang, D. X.; Piner, R.; Velamakanni, A.; Jung, I.; Tutuc, E.; Banerjee, S. K.; Colombo, L.; Ruoff, R. S. Large-Area Synthesis of High-Quality and Uniform Graphene Films on Copper Foils. *Science* **2009**, *324*, 1312-1314.

10. Malard, L. M.; Pimenta, M. A.; Dresselhaus, G.; Dresselhaus, M. S. Raman Spectroscopy in Graphene. *Phys. Rep.* **2009**, *473*, 51-87.

11. Reina, A.; Jia, X.; Ho, J.; Nezich, D.; Son, H. B.; Bulovic, V.; Dresselhaus, M. S.; Kong, J. Large Area, Few-Layer Graphene Films on Arbitrary Substrates by Chemical Vapor Deposition. *Nano Lett.* **2009**, *9*, 30-35.

19

12. Sun, Z.; Raji, A.-R. O.; Zhu, Y.; Xiang, C. S.; Yan, Z.; Kittrell, C.; Samuel, E. L. G.; Tour, J. M. Large-Area Bernal-Stacked Bi-, Tri-, and Tetralayer Graphene. *ACS Nano* **2012**, *6*, 9790-9796.

13. Yamashita, T.; Hayes, P. Analysis of XPS Spectra of Fe^{2+} and Fe^{3+} Ions in Oxide Materials. *Appl. Surf. Sci.* **2008**, *254*, 2441-2449.

14. Dhavale, V. M.; Singh, S. K.; Nadeema, A.; Gaikwada, S. S.; Kurungot, S. Nanocrystalline $Fe-Fe_2O_3$ Particle-Deposited N-Doped Graphene as an Activity-Modulated Pt-Free Electrocatalyst for Oxygen Reduction Reaction. *Nanoscale* **2015**, *7*, 20117-20125.

15. Dresselhaus, M. S.; Jorio, A.; Hofmann, M.; Dresselhaus, G.; Saito, R. Perspective on Carbon Nanotubes and Graphene Raman Spectroscopy. *Nano Lett.* **2010**, *10*, 751-758.

16. Hertel, S.; Waldmann, D.; Jobst, J.; Albert, A.; Albrecht, M.; Reshanov, S.; Schoner, A.; Krieger, M.; Weber, H. B. Tailoring the Graphene/Silicon Carbide Interface for Monolithic Wafer-Scale Electronics. *Nat. Commun.* **2012**, *3*, 957.

17. Xu, H. T.; Wang, S.; Zhang, Z. Y.; Wang, Z. X.; Xu, H. L.; Peng, L. M. Contact Length Scaling in Graphene Field-Effect Transistors. *Appl. Phys. Lett.* **2012**, *100*, 103501-103504.

18. Nagashio, K.; Nishimura, T.; Kita, K.; Toriumi, A. Contact Resistivity and Current Flow Path at Metal/Graphene Contact. *Appl. Phys. Lett.* **2010**, *97*, 143514-143516.

19. Wang, L.; Meric, I.; Huang, P. Y.; Gao, Q.; Gao, Y.; Tran, H.; Taniguchi, T.; Watanabe, K.; Campos, L. M.; Muller D. A.; Guo, J.; Kim, P.; Hone, J.; Shepard, K. L.; Dean, C. R. One-Dimensional Electrical Contact to a Two-Dimensional Material. *Science* **2013**, *343*, 614-620.

20

20. Song, S. M.; Kim, T. Y.; Sul, O. J.; Shin, W. C.; Cho, B. J. Improvement of Graphene-Metal Contact Resistance by Introducing Edge Contacts at Graphene under Metal. *Appl. Phys. Lett.* **2014**, *104*, 183506-183508.

21. Léonard, F.; Talin, A. A. Electrical Contacts to One- and Two-Dimensional Nanomaterials. *Nat. Nanotechnol.* **2011**, *6*, 773-783.

22. Lee, S. K.; Kabir, S. M. H.; Sharma, B. K.; Kim, B. J.; Cho, J. H., Ahn, J. H. Photo-Patternable Ion Gel-Gated Graphene Transistors and Inverters on Plastic. *Nanotechnology* **2014**, *25*, 014002-014007.

23. Das, A.; Pisana, S.; Chakraborty, B.; Piscanec, S.; Saha, S. K.; Waghmare, U. V.; Novoselov, K. S.; Krishnamurthy, H. R.; Geim, A. K.; Ferrari, A. C. Monitoring Dopants by Raman Scattering in an Electrochemically Top-Gated Graphene Transistor. *Nat. Nanotechnol.* **2008**, *3*, 210-215.

24. Sun, S.; Zeng, H. Size-Controlled Synthesis of Magnetite Nanoparticles. *J. Am. Chem. Soc.* **2002**, *124*, 8204-8205.

TOC graphic